A Neuromorphic Prosthesis to Restore Communication in Neuronal Networks

Stefano Buccelli, Yannick Bornat, Ilaria Colombi, Matthieu Ambroise, Laura Martines, Valentina Pasquale, Marta Bisio, Jacopo Tessadori, Przemyslaw Nowak, Filippo Grassia, et al.

A neuromorphic prosthesis to restore communication in neuronal networks

Stefano Buccelli[1,2,3#], Yannick Bornat[4#], Ilaria Colombi[2,3$], Matthieu Ambroise[4$], Laura Martines[2,3$], Valentina Pasquale[3], Marta Bisio[3,5], Jacopo Tessadori[3,6], Przemysław Nowak[2,7], Filippo Grassia[4,8], Alberto Averna[1,2,3], Mariateresa Tedesco[2], Paolo Bonifazi[9,10,11], Francesco Difato[3], Paolo Massobrio[2], Timothée Levi[4,12]*& Michela Chiappalone[1,3]*^

[#]These authors contributed equally;

[$]These authors contributed equally;

*Corresponding authors

Affiliations

1 Rehab Technologies IIT-INAIL Lab, Istituto Italiano di Tecnologia, Via Morego 30, 16163 Genova, Italy;

2 Department of Informatics, Bioengineering, Robotics, System Engineering (DIBRIS), University of Genova, Via all'Opera Pia 13, 16145, Genova, Italy;

3 Department of Neuroscience and Brain Technologies, Istituto Italiano di Tecnologia, Via Morego 30, 16163, Genova, Italy;

4 Laboratoire de l'Intégration du Matériau au Système (IMS), University of Bordeaux, Bordeaux INP, CNRS UMR 5218, 351 Cours de la Libération, 33405 Talence Cedex, France;

5 Department of Neurosciences, University of Padova, Via Nicolò Giustiniani 5, 35128, Padova, Italy;

6 Department of Advanced Robotics, Istituto Italiano di Tecnologia, Via Morego 30, 16163 Genova, Italy;

7 Institute of Information Technology, Lodz University of Technology, ul. Wolczanska 215, 90-924, Lodz, Poland;

8 University of Picardie Jules Verne, Laboratory of Innovative Technologies (LTI, EA 3899), Avenue des Facultés, Le Bailly, 80025 Amiens, France;

9 School of Physics and Astronomy, Tel Aviv University, 69978 Tel Aviv, Israel;

10 Computational Neuroimaging Laboratory, Biocruces Health Research Institute, Hospital Universitario Cruces, 48903, Baracaldo, Vizcaya, Spain

11 Ikerbasque: The Basque Foundation for Science, 48013 Bilbao, Bizkaia, Spain

12 LIMMS CNRS-IIS, The University of Tokyo, 153-8505 Tokyo, Japan

^Lead Contact

Dr Michela Chiappalone, PhD

Rehab Technologies IIT-INAIL Lab, Istituto Italiano Di Tecnologia, Via Morego 30, 16163 Genova

Tel: +39 010 71781743

E-mail: michela.chiappalone@iit.it

***Corresponding authors**

Dr Michela Chiappalone, PhD

Rehab Technologies IIT-INAIL Lab, Istituto Italiano Di Tecnologia, Via Morego 30, 16163 Genova

Tel: +39 010 71781743

E-mail: michela.chiappalone@iit.it

Associate Prof Timothée Levi, PhD

Laboratoire de l'Intégration du Matériau au Système (IMS), University of Bordeaux, Bordeaux INP, CNRS UMR 5218, 351 Cours de la Libération, 33405 Talence Cedex

Tel: +33 54000 3118

E-mail: timothee.levi@u-bordeaux.fr

LIMMS, CNRS–Institute of Industrial Science, UMI 2820, The University of Tokyo,

4-6-1 Komaba, Meguro-ku, Tokyo, 153-8505, Japan

Tel: +81 3 5452 6721

E-mail: levi@iis.u-tokyo.ac.jp

Summary

Recent advances in bioelectronics and neural engineering allowed the development of brain machine interfaces and neuroprostheses, capable of facilitating or recovering functionality in people with neurological disability. To realize energy-efficient and real-time capable devices, neuromorphic computing systems are envisaged as the core of next-generation systems for brain repair. We demonstrate here a real-time hardware neuromorphic prosthesis to restore bidirectional interactions between two neuronal populations, even when one is damaged or missing. We used *in vitro* modular cell cultures to mimic the mutual interaction between neuronal assemblies and created a focal lesion to functionally disconnect the two populations. Then, we employed our neuromorphic prosthesis for *bidirectional bridging* to artificially reconnect two disconnected neuronal modules, and for *hybrid bidirectional bridging* to replace the activity of one module with a real-time hardware neuromorphic Spiking Neural Network. Our neuroprosthetic system opens avenues for the exploitation of neuromorphic-based devices in bioelectrical therapeutics for healthcare.

Keywords:

In vitro neuronal networks; micro-electrode arrays; real-time signal processing; closed-loop; neurobiohybrid; brain repair.

Introduction

One of the greatest challenges of modern neuroscience is to find reliable and sustainable treatments for the disabling effects caused by many chronic and incurable brain conditions. With the greatest impact carried by stroke (Feigin et al. 2017) and traumatic brain injury (Maas et al. 2017), brain disorders are among the leading causes of disabilities worldwide. Due to recent advances in bioelectronics and in neural and neuromorphic engineering, direct interfacing of artificial circuits with large neuronal networks is possible to develop novel 'neurobiohybrid' systems (such as neuroprostheses (Vassanelli and Mahmud 2016)), which are envisaged as potentially interesting clinical applications for brain lesions (Broccard et al. 2017). In this paper, we introduce an innovative bioelectronic system acting as a neuroprosthesis which, thanks to a neuromorphic real-time hardware interface, can re-establish the communication between two disconnected neuronal populations.

Neural interfaces are promising solutions for brain repair (Soekadar et al. 2015). Modern neural interfaces are mainly designed to restore lost motor functions in only one direction, i.e., from the brain to the body (Abdulkader et al. 2015) or from the body to the brain (Flesher et al. 2016). Additionally, recent neuroprosthetic developments have shown the enormous potential of neural interfaces to aid and accelerate functional recovery (Bouton et al. 2016; Rosin et al. 2011). However, a major obstacle in developing novel neuroprostheses for bidirectional communication with and within the brain is the complex nature of interactions among different brain areas, which in turn presents a challenge for the development of appropriate stimulation protocols as well as for testing such devices using *in vivo* models (Kohler et al. 2017).

Despite very recent technological progress (Jun et al. 2017; Steinmetz et al. 2018), *in vivo* models still have two main bottlenecks. The first bottleneck is the technical challenge to faithfully reproduce specific/focal network lesions (mainly due to their complexity) that the

neuroprosthesis aims to treat, whereas the second is the difficulty in disentangling the actual effect of the adopted electrical therapy from the complex activity of a brain constantly processing sensory inputs and producing behaviour. Therefore, since *in vivo* models exhibit inherent complexity and low controllability, using *in vitro* reduced neuronal systems to model precise and reproducible neuronal network lesions and test neuroprosthetic devices for their treatment may be advantageous. This approach is also justified by a growing recognition that *in vitro* testing of both research and medical devices can be more effective in terms of cost, time consumption and ethical issues and much more reliable than *in vivo* testing (Myers et al. 2017).

In this work, we bidirectionally interfaced in real-time a neuroprosthetic system with an *in vitro* culture constituted by interconnected 'neuronal assemblies' (Hebb 1949). Therefore, our first objective was to create a simplified yet plausible *in vitro* model of a focal brain lesion by using bimodular cultures grown onto micro-electrode arrays (MEAs) (Bisio et al. 2014; Bonifazi et al. 2013; Shein-Idelson et al. 2011) with reciprocal connections cut by a custom-made laser setup (Difato et al. 2011) to mimic the pathological effect of a traumatic brain injury (Hayes et al. 2016). We created a neurobiohybrid system connecting the biological element (the bimodular culture) following the lesion with a neuroprosthetic prototype. Our hardware neuroprosthesis could perform low-power computations in hard real-time (Pirog et al. 2018), collecting the inputs coming from neural recordings, processing those signals and generating suitable electrical stimulation triggers as an output. With this experimental setup, we tested two specific applications, namely, *bidirectional bridging* (BB) to artificially reconnect two disconnected neuronal modules and *hybrid bidirectional bridging* in which a real-time spiking neural network (SNN) replaced the activity of one of the two modules in real-time while implementing bidirectional connectivity with the remaining neuronal module.

The motivation of our research is to provide a new technological instrument as a novel form of neuroprosthesis aimed at treating disabling brain pathologies. The hardware choice (field-programmable gate array, FPGA) maximise the real-time performances of the system and allows for a faster development of a future implantable biolectronic device for biomedical applications. The adoption of bidirectional communication allows the development of a generalized non-specific approach that is applicable to the central nervous system (CNS) or peripheral nervous system. In particular, prostheses for the CNS should restore the communication between two or more neuronal assemblies whose functional and anatomical path could be distributed and sparse and not necessarily known *a priori*.

Indeed, our idea to develop a generalized approach comes from the future perspective of creating a cerebral neuroprosthesis for direct implantation in the brain that could be used by patients affected by stroke or brain injury. Our proof-of-principle results are the first for a next-generation neurobiohybrid system to restore brain functions (Broccard et al. 2017; Vassanelli and Mahmud 2016).

Results

Neuroprosthetic architecture

To create bimodular *in vitro* systems, we developed PDMS masks with two connecting compartments that constrained the growth of neuronal cells in two precise areas over 60-electrode MEAs (Figure S1). The obtained bimodular neuronal culture constitutes the biological neuronal network (BNN) of our system (Figure 1A). The signal from the BNN was amplified by a commercial system and acquired by a custom-developed FPGA-based neuromorphic board (Figure S2) previously configured by a custom-made MATLAB code (MathWorks, Natick, MA, USA) running on a general purpose personal computer. The neuromorphic board triggered a commercial stimulator to close the loop with the BNN. The general protocol designed for this study involved three steps. First, spontaneous activity in both neuronal modules was recorded ('pre-lesion condition'). Then, laser ablation of the biological connections between the two modules was performed (see Transparent Methods), followed by recording of spontaneous activity in both modules ('post-lesion condition') to assess the viability of the networks. Finally, we tested our neuroprosthetic device using two experimental frameworks. In the first case, we applied a reconnection strategy using a bidirectional activity-dependent stimulation ('bidirectional bridging', BB), whereas in the second case, we interfaced a hardware-implemented biomimetic SNN with one of the two neuronal modules ('hybrid bidirectional bridging', HBB) to simulate a 'replacement' strategy that utilizes the bidirectional interaction between the biological system and its artificial counterpart (Figure 1B). The sequence of algorithms (e.g., spike detection, network burst detection) implemented on the board to realize both experimental approaches (BB or HBB) is schematically depicted in Figure 1C.

<FIGURE 1 ABOUT HERE>

Control experiments

To evaluate the stability and effect of the focal lesion on bimodular BNN activity, we first performed two sets of control experiments. In the first set defined as 'experiments with no lesion' (Figure 2A1), we recorded 4 consecutive hours of spontaneous activity (S1-S4, n=9 cultures). In the second set defined as 'experiments with a lesion' (Figure 2A2), we recorded one hour of spontaneous activity (S1), followed by laser ablation of the connections between the two modules, which usually took less than 20 minutes. Next, we recorded 3 hours of spontaneous activity post lesion (SPL1-SPL3) to quantify the effects of laser ablation (n=4 cultures). As depicted in the raster plot of one representative experiment (Figure 2B1), bimodular neuronal networks exhibited spontaneous, synchronized, multi-unit activity composed of network-wide bursts (NBs) spreading over the two modules. Following laser ablation, the propagation between compartments was disrupted, as shown in Figure 2B2.

With no lesion, the percentage of active channels with respect to the first hour of recording (S1) was higher than 98% and was maintained for the entire duration of the experiment (Figure 2D1, light blue bars). The mean firing rate (MFR) was stable for all control experiments with no lesion (from S1 to S4, Figure S3 A). Alternatively, control experiments with lesions showed a reduced number of active channels (close to 73%) during the first hour after ablation (SPL1). During the following two hours (SPL2-SPL3), this value increased and reached 93% at the end of the recording (Figure 2C1, dark grey bars). No significant differences were found. The MFR was quite stable for all control experiments with lesions except between S1 and SPL1 (Figure S4 A). The activity level with respect to the S1 phase, expressed by the MFR ratio with respect to S1, was stable during the control experiments without lesions (Figure 2D2, light blue bars). The lesion produced a clear

192 decrease in activity in most cultures, especially during the first two hours (SPL1-SPL2,
193 Figure 2D2). We found a significant difference between the two experimental sets during the
194 first two hours after S1 but not during the last hour. This result suggests that two hours after a
195 lesion, almost complete spontaneous recovery occurred in terms of the firing rate for the two
196 neuronal modules.

197 To evaluate changes in the synchronicity between the two modules, we performed
198 cross-correlation (CC) analysis between the collapsed spike trains of each module. The shape
199 of the CC function was stable throughout the entire recordings in experiments without
200 lesions, as reported in Figure 2C1 for a representative experiment. After a lesion, the CC
201 function collapsed to zero and did not recover during the experiment (Figure 2C2:
202 representative experiment). To quantify this difference, we integrated the CC function in a
203 range of ±500 ms to obtain the CC area. We did not find any significant change in the CC
204 area values for all experiments with no lesion (Figure S3B). By contrast, the CC area values
205 showed a marked decrease following the lesion (SPL1). This decrease was due to the lack of
206 anatomical connections between the compartments and did not recover by itself (Figure
207 S4B). Comparing the CC area ratio between later phases and S1 resulted in a significant
208 difference between matching periods in 'lesion' and 'no lesion' experiments (Figure 2E1).
209 We also computed the correlation coefficient (i.e. Pearson Correlation, PC) among all the
210 active channels both intra module and inter module (Figure 2E2). The intra-module PC was
211 constant across experimental phases for controls with no lesion (light blue bars). On the other
212 hand, for controls with lesion (dark grey bars) there was a drop in the intra-module PC,
213 related to the reduced firing rate following the lesion, but no statistical difference was found
214 (Figure 2E2, left panel). The inter-module CC was stable for controls with no lesion. On the
215 other hand, following the lesion the inter-module PC collapsed and never recovered by itself
216 (Figure 2E2, right panel) as already demonstrated with the previous analysis.

The network bursting rate (NBR) was stable during all experiments with no lesions (Figure S3C). For the experiments with lesions, this parameter was less stable but with no significant differences between phases (Figure S4C). When comparing the two experimental protocols with the NBR ratio with respect to S1, we found significant differences during the first and the second hour post lesion (Figure 2F1). The mean probability to have NBs composed of spikes belonging to a single module (i.e. Prob smNB, see Transparent Methods) was close to 0.2 in the experiments without lesions (Figure S3D), meaning that the majority of NBs in an intact bimodular network involved both modules. Alternatively, following the lesion, the probability became close to 1 (Figure S4D), meaning a total loss of functional communication between the two compartments. Using the Prob smNB ratio with respect to S1 (Figure 2F2), we found significant differences between the two experimental groups during all phases post lesion (Mann-Whitney test; $p < 0.05$). Thus, for the no lesion experiment, the Prob smNB remained very similar to the initial values, while for the lesion experiments, it changed abruptly due to the lesion. This result further confirmed that the lesion was effective in functionally disconnecting the two modules.

< FIGURE 2 ABOUT HERE >

Experiment 1: Bidirectional Bridging (BB)

The goal of this experiment is to restore communication between two neuronal assemblies after lesion-induced separation. To achieve this goal, we designed and implemented a stimulation reactive paradigm inspired by the 'activity-dependent stimulation' (ADS) described in (Guggenmos et al. 2013) in our neuromorphic board. In contrast to the control experiments, the general protocol (Figure 3A) included 20 minute recordings of spontaneous activity before the lesion (S1). Upon the lesion execution, we waited for two hours to reach

242 stable activity in both modules, as shown by the results of control experiments (see Figure 2).
243 Then, we recorded 20 minutes of spontaneous activity (SPL3). The raster plot of a
244 representative experiment is reported in Figure 3b. Before the lesion (S1), the bursting
245 activity involved both modules (Figure 3B1), whereas after the lesion (SPL3), the activity
246 was characterized by single-module NBs (Figure 3B2). To choose the best parameters
247 (threshold and window time, see Transparent Methods) that allowed us to reliably detect NBs
248 in both modules, we performed offline NB detection. After the FPGA was updated with these
249 parameters, a 20 minute session of BB was conducted. (see, Figure 1B and C for the
250 description of the BB protocol). The BB approach implemented a reactive paradigm: every
251 time an NB was detected in one module, a stimulation pulse was delivered to an electrode in
252 the other module (see Transparent Methods) in both directions. During the BB phase, the
253 bursting activity involved both modules similar to the intact condition due to the bidirectional
254 stimulation pulses (Figure 3B3, blue and red lines represent electrical stimulation pulses
255 delivered from module 1 to module 2 and vice versa). The last phase of the protocol involved
256 20 additional minutes of spontaneous activity (SPL4), which showed the same activity as
257 SPL3 (Figure 3B4). We did not observe significant changes in spiking activity (i.e., MFR)
258 throughout the recordings (Figure 3c).
259 Next, we evaluated the effect of this configuration in terms of CC (Figure 3d1and 2).
260 During spontaneous activity before the lesion (S1), the CC peak was high and stable due to
261 the functional and anatomical connections between the two modules, which was also reported
262 for the control experiments. After the lesion (SPL3), there was a decrease in CC that was not
263 expected to recover without external intervention, as we demonstrated before (see, Figure
264 2D). The bidirectional stimulation at least partially recovered the CC area and consequently
265 the communication between modules (Figure 3D2), as demonstrated by statistical analysis.
266 Regarding the number of NBs, we did not find any significant difference between the

experimental phases (Figure 3E1). However, the probability of isolated NBs was not uniform; it reached the maximum value after the lesion, as we previously observed in the control experiments with lesions (see, Figure 2D2). During bidirectional stimulation, these values became closer to the spontaneous recording (Figure 3E2), meaning that NBs mainly involved both modules. This finding further confirmed that the BB protocol could reconnect two disconnected modules though a real-time ADS acting in both directions (from module 1 to module 2 and from module 2 to module 1).

<FIGURE 3 ABOUT HERE>

Experiment 2: hybrid bidirectional bridging (HBB)

With an injury causing damage to an entire neuronal subnetwork, a reconnection strategy such as the BB illustrated above would not be feasible. For this reason, we developed a second reconnection strategy based on the use of a hardware SNN that can interact in real-time with its biological counterpart, HBB (see Figure 1). We created a set of SNNs (i.e., SNN library) by tuning the mean value of the synaptic weight distributions of our models to cover the variability of the BNNs (i.e., BNN library, Figure 4A). The biomimetic SNN (see Figure S5), working in hardware real-time to allow bidirectional communication with living neurons, was modelled as a network of 100 Izhikevich (IZH) neurons (Izhikevich 2003), with 80 excitatory and 20 inhibitory neurons (see Transparent Methods), according to the biological composition of dissociated cultures (Bonifazi et al. 2005; Hayashi et al. 2003). Synaptic noise (Grassia et al. 2016), inhibitory and excitatory synapses (Izhikevich 2004), short-term plasticity (Izhikevich and Edelman 2008) and axonal delays were included in the model to recreate the network dynamics (see Transparent Methods and Figure S6 A1 and A2). Regarding the connectivity rules, we set the outdegree (i.e., the number of post-synaptic

neurons) to 25 for all neurons in the network, while the indegree (i.e., the number of pre-synaptic neurons) followed a normal distribution with a mean value of 25 and a standard deviation of 4.3 (Figure S6, R-Square=0.806). The goal of creating an SNN library was to cover a wide range of NBRs because NB was chosen as the triggering event for our reconnection paradigm, as explained above. To this end, we tuned only the mean value of the normal distribution of synaptic weights (the standard deviation was kept constant at the value of 0.3). By increasing or decreasing the mean synaptic weights, we tuned the NBR. For excitatory synapses, the mean value ranged from 0.99 to 1.34 (Figure 4C left), while that for inhibitory synapses ranged from -2.02 to -1.02 (Figure 4C right and Table S1). As previously stated, our goal was to cover the NBR variability and not the MFR. The MFR variability in our BNN library was higher than that obtained with our SNN library (Figure 4E and F1). Nevertheless, the BNN variability in terms of NBR was completely covered by our SNN library, which also contains networks with a much higher NBR than that in the BNN library (Figure 4F2).

<FIGURE 4 ABOUT HERE>

The general HBB protocol (Figure 5A) is similar to the BB protocol. The HBB procedure included a 20 minute recording of spontaneous activity before the lesion. This recording was used to quantify activity in terms of the NB rate of the network. This feature was used to choose one SNN from the SNN library that had an NB rate closer to its biological counterpart. We waited two hours after the lesion to allow activity in both modules to stabilize, as shown by the results of control experiments (e.g., Figure 2). Then, we recorded 20 minutes of spontaneous activity. After setting FPGA detection parameters, we performed a 20 minute HBB session (see, Figure 1B and C for the description of the HBB protocol). As anticipated, the HBB approach also implemented an ADS paradigm; every time an NB was

detected on the 'surviving' module (i.e., when one of the two modules was completely damaged), a stimulation pulse was delivered to the SNN. The board implemented the corresponding paradigm in the opposite direction. Detection of NBs occurred in the SNN, while stimulation was delivered to the 'surviving' module, thus avoiding the imposition of any predefined unidirectional communication. Next, we recorded 20 additional minutes of spontaneous activity.

We did not observe significant changes in terms of spiking activity (i.e., MFR) throughout the recordings (Figure 5C). Then, we evaluated the effect of this configuration in terms of CC (Figure 5D1 and 2). During spontaneous activity before the lesion (S1), the CC peak was high and stable due to the functional and anatomical connections between the two modules, which was also reported for the control experiments. As expected, with no external intervention, CC decreased sharply after the lesion (SPL3), as we previously observed. One of the two modules was damaged, while the correlation was evaluated between the SNN and the surviving module during the HBB phase. The bidirectional stimulation created a relevant correlation area between SNN and the surviving module, as demonstrated by statistical analysis. Regarding the number of NBs, we did not find a significant difference between the S1 and HBB phases (Figure 5E1). However, the probability of isolated NBs was not uniform; it reached the maximum value after the lesion, as we previously observed in the control experiments with lesions (see, Figure 3E2). During the hybrid bidirectional stimulation, these values became closer to the spontaneous recording (Figure 5E2), meaning that NBs mainly involved both modules. This finding further confirmed that the HBB protocol created a hybrid system with the surviving biological module though real-time ADS acting in both directions (from BNN to SNN and from SNN to the BNN).

<FIGURE 5 ABOUT HERE>

Discussion

We presented an innovative neuromorphic prosthesis based on a FPGA board and demonstrated two successful reconnection paradigms for a lesion interrupting the communication between two neuronal populations *in vitro*.

According to previous reports, *in vitro* systems constitute a successful experimental model of neuronal dynamics (Javier et al. 2013; Johnson et al. 2010), thus providing an excellent test bed for adaptive closed-loop neural interfaces (Potter 2010). Starting from our recently developed methodology (Kanner et al. 2015), we created custom bimodular cultures with the goal of reproducing two interacting neuronal populations, thus mimicking the intrinsic modularity of the brain (Bonifazi et al. 2013). Our bimodular cultures were highly temporally stable in terms of firing properties at the whole network level as the activity between the two populations remained highly correlated for the entire duration of the recording. A lesion produced via laser ablation was employed to physically cut the connections between the two modules. This methodology was proven to be safe because it produced localized damage by selectively ablating subcellular compartments without damaging adjacent structures (Difato et al. 2011; Habibey et al. 2015; Soloperto et al. 2016). We assume that such a focal damage, allowing to specifically cut few connections among those available in the network, together with possible intrinsic compensatory mechanisms of synaptic scaling (le Feber et al. 2017; Turrigiano 2008), were responsible of the spontaneous recovery of the firing rate on a timescale of two-three hours. This demonstrates the effectiveness of our technique in preserving the functionality of the two modules while decoupling their activity, as proven by the loss of correlation of bursting behaviour.

Two different applications of our neuroprosthesis, BB and HBB, were tested. Our neuromorphic prosthesis, independently of the stimulation paradigm, works according to a closed-loop reactive policy as follows: each time a condition is met (i.e., an ‘event’ is

368 detected), a stimulus is delivered. The hardware architecture was designed to be flexible
369 enough to allow the implementation of different experimental paradigms and the definition of
370 different triggering events. In our study, we chose 'NBs' as trigger events (see Transparent
371 Methods). The choice to deliver a stimulation depending on a network-wide event has two
372 main advantages as follows: first, NB frequency is low enough to avoid inducing plasticity
373 phenomena by electrical stimulation in our cultures (Wagenaar et al. 2006), which could
374 confound the final results and effectiveness of neuroprosthetic reconnection. The second
375 point is anticipation of the following major issue that will emerge during *in vivo* recordings:
376 monitoring single neurons presents problems at both theoretical (Guggenmos et al. 2013) and
377 practical levels. Namely, how much information on complex functions can be obtained by
378 single-neuron observation remains unclear (Luczak et al. 2015; Panzeri et al. 2017), while
379 tracking the activity of the same neuron for extended periods of time is problematic (Kozai et
380 al. 2015). Taking multiple input sources into account was also used in the work of Berger
381 (Berger et al. 2012), but they employed a neuroprosthetic strategy different from ours. In
382 particular, these authors used a generalized linear model to predict the CA1 activity from
383 spikes in CA3 of the hippocampal circuit. Our system is considered more flexible and
384 adaptable to networks with different connectivity, not just feedforward similar to that in the
385 hippocampus. Moreover, we were interested in mimicking the overall spiking activity of the
386 network and not mapping an input-output transformation only.
387 Another important novelty of our system regards directionality. To our best
388 knowledge, this neuroprosthetic system is the first to implement a truly bidirectional
389 interaction with a SNN through a hard real-time interface. We recorded activity from the first
390 module (via multiple sources); when a criterion was met, the device stimulated the second
391 module (this is how a 'typical' closed-loop in neuroscience works, for a review see
392 (Greenwald et al. 2016)). The novelty is simultaneously monitoring multiple sources from

another module and delivering the stimulation when the triggering event is detected. To date and as far as we are aware of, only Jung and colleagues (Jung et al. 2001) have performed a bidirectional interface to a neuromorphic device, but their models were not precise at the spike level (modelling neuron populations) and they used non configurable analogue electronics, which resulted in an experiment-specific setup. The other neuroprosthetic devices that have been proposed in the literature can implement a 'unidirectional' artificial link only from one area to another (or maybe the same) but not doubling it. Here, we are not imposing any preferred directionality to the communication; networks are self-organizing on the basis of their intrinsic natural relationship (we are not imposing who is driving whom). This approach has the main advantage of informing both brain regions (i.e., neuronal modules, in our case) that an event occurred in the other region, given that interaction in the brain is intrinsically bidirectional (Roelfsema and Holtmaat 2018). For example, in the sensorimotor system, sensory simulation can help motor recovery (Cuppone et al. 2018), and motor learning can enhance sensory functions (Ostry et al. 2010; Takeuchi and Izumi 2013). Applications of our neuroprosthetic systems to conditions where the sensorimotor interaction is impaired would allow restoration of both communication channels, suggesting improvements in current rehabilitation therapies. Moreover, although tested on a bimodular system, the neuromorphic FPGA board can be easily upgraded to play the bridging role on an arbitrary number (within reason) of different neuronal circuits. A recent work (Forró et al. 2018) developed directional networks of primary hippocampal neurons on MEA and compared the information flow of these networks with respect to bidirectional networks (similar to our bimodular preparations). They found that without physically imposing a unidirectional configuration, there is a continuous back and forth communication between nodes thus suggesting the importance of a bidirectional communication in a healthy network.

The second paradigm we tested was based on the use of a biomimetic SNN to 'substitute' a missing/damaged neuronal population. Currently, SNN applications span different fields, including computational neuroscience (Markram 2012; Melozzi et al. 2017), and very recently, they were used for sensory encoding in hand prosthesis for amputees (Osborn et al. 2018; Valle et al. 2018). SNNs can be simulated in software (Goodman and Brette 2009) and/or neuromorphic hardware (Thakur et al. 2018). As time and energy consumption are fundamental in neuroprosthetic applications for translational purposes, the use of hardware-based computing systems becomes mandatory.

In general, hybrid systems composed of *in vitro* BNNs coupled to SNNs are rare. In one approach, the SNN served as a self-organizing classifier of activity patterns exhibited by the BNN, with output of the SNN being subsequently used to control the behaviour of a robot (Pizzi et al. 2009). Other studies focused on the unidirectional or bidirectional influence of the two networks, investigating the dynamics of the interaction between the BNN and SNN in which the SNN played a role of an artificial counterpart of its biological original (Bruzzone et al. 2015; Chou et al. 2015). However, closed-loop effects in those hybrid networks were not thoroughly determined. In one of these studies, only unidirectional connectivity was considered with input from the SNN to the BNN, which was also simulated beforehand (Bruzzone et al. 2015). In this study, we established hybrid communication in the case of an entire neuronal population that needed substitution.

A study by Chou *et al*. (Chou et al. 2015) implemented a bidirectional interface between an SNN and a retinal slice obtained from an adult rat and recorded by an MEA. This system is quite interesting, but there is a 1 s delay between the BNN and SNN interactions. Therefore, this delay in Chou's setup is 3 orders of magnitude larger than that in our work in which the sampling of biological activity is never interrupted, and the step size of the SNN is 1 ms. The difference between the two systems is radical; bidirectional communication in real-

time allows actual clinical application, whereas delays in the range of seconds prevent (or at least seriously reduce) the possibility of meaningful control of a biological system.

A recent study, inspired by a previous work (Hogri et al. 2015), implemented a hybrid interaction (Xu et al. 2018) between the cerebellum of a rat and an SNN implemented on FPGA. Their model involved 10k leaky integrate and fire (LIF) neurons and did not integrate other biomimetic behaviours, such as axonal delay, short-term plasticity and synaptic noise, unlike the IZH neurons implemented in our system. Both the hard real-time processing and simplified neuronal model (which allow mimicking the richness of the electrophysiological patterns *in vivo*) are mandatory for reproducing the biological dynamics of living neural networks and for performing useful real-time hybrid experiments.

In this work, we demonstrated the possibility to design a neuromorphic all-hardware prosthesis capable of artificially reconnect two disconnected neuronal networks or artificially replacing one entire neuronal sub-network.

The use of a fully integrated hardware computing system allowed hard real-time performances and low power consumption, which are crucial for translational purposes related to therapeutic applications in humans (Kipke et al. 2008; Wang et al. 2010).

Limitations of the study

A limitation of the present work is that we deliberately chose to downsample both the number of biological neurons recorded through a low density MEA and the number of artificial neurons implemented on the FPGA. For the purpose of detecting network-wide activity, this oversimplification of biological complexity can be acceptable to test the functionality of the device and the feasibility of the approach, but if the goal is to functionally replace a biological network, a higher resolution would be preferable. It is worth underlying that this hardware implementation is not exploiting the full resources of the FPGA, thus in

follow-up studies, also thanks to the flexibility of our system, we foresee to scale up the number of neurons and synapses and to upgrade the computational algorithms to deal with more complex experimental designs. From a technological point of view, the current state of the art makes possible the use of devices with a large number (thousands) of recording electrodes (Berdondini et al. 2009; Frey et al. 2009). Such an improvement would also allow to have more information about functional connectivity of the biological network (Pastore et al. 2018) and thus developing more realistic, in terms of topology, artificial models. In this work, we arbitrarily modeled the network connectivity with a random adjacency matrix since the use of MEAs with 60 electrodes made impossible to correctly identify the topological properties (e.g., hubs, recurring connections, modules, etc.) of the network under investigation.

We are aware that the road is still long to target human applications. Despite this, we think that the extensive work performed represent an important milestone to start from. The next fundamental (and critical) step would be to test the neuromorphic prosthesis in vivo, for example on animal models affected by ischemic or traumatic lesions (Guggenmos et al. 2013). Even if the adaptation to the new experimental set-ups will require time, we believe these are necessary steps to further push the translational potential of our system, which will be able to create real innovation in the clinical therapeutics.

Acknowledgements

The presented research results has received funding from the European Union's Seventh Framework Programme (ICT-FET FP7/2007-2013, FET Young Explorers scheme) under grant agreement n° 284772 BRAIN BOW (www.brainbowproject.eu).

The authors would like to thank: Dr Daisuke Ito, Dr Marina Nanni, Dr Claudia Chiabrera, and Dr Giacomo Pruzzo for precious technical support in performing the *in vitro* experiments at IIT. The authors are grateful to Dr Marianna Semprini for useful comments on the final drafts of the manuscript. The authors wish to thank Prof. Sergio Martinoia, Prof. Sylvie Renaud, Prof. Sylvain Saighi and Prof. Ari Barzilai for their mentorship during the BrainBow project and for useful discussions on the final results.

Author contributions

T. L., Y. B., P. M., P. B. and M. C. designed the study. Y. B. and T. L. designed and fabricated the hardware board. S. B., V. P., F. D., and M. C. designed the experiments. M. A., P. M., P. N., F. G. and T. L. designed and worked on SNN. I. C., M. B., and M. T. prepared the bimodular cultures. S. B., L. M., A. A. and F. D. performed the experiments. S. B., L. M., J. T., V. P., and M. C. designed the analyses. S. B. and L. M. performed the analyses. S. B., I. C., and V. P. performed the statistical analyses. S. B. and I. C. prepared the original figures. S. B., I. C., T. L., and M. C. wrote the manuscript. T. L., P. M., P. B. and M. C. acquired funding to conduct the research. All authors have read, corrected and approved the final version of the manuscript.

Declaration of Interests

The Authors report no competing interests.

References

Abdulkader, S.N., Atia, A., Mostafa, M.-S.M., 2015. Brain computer interfacing: applications and challenges. Egypt. Inform. J. 16(2), 213–230.

Berdondini, L., Imfeld, K., Maccione, A., Tedesco, M., Neukom, S., Koudelka-Hep, M., Martinoia, S., 2009. Active pixel sensor array for high spatio-temporal resolution electrophysiological recordings from single cell to large scale neuronal networks. Lab on a chip 9(18), 2644-2651.

Berger, T.W., Song, D., Chan, R.H., Marmarelis, V.Z., LaCoss, J., Wills, J., Hampson, R.E., Deadwyler, S.A., Granacki, J.J., 2012. A hippocampal cognitive prosthesis: multi-input, multi-output nonlinear modeling and VLSI implementation. IEEE Trans. Neural Syst. Rehabil. Eng. 20(2), 198–211.

Bisio, M., Bosca, A., Pasquale, V., Berdondini, L., Chiappalone, M., 2014. Emergence of bursting activity in connected neuronal sub-populations. PLoS One 9(9), e107400.

Bonifazi, P., Difato, F., Massobrio, P., Breschi, G.L., Pasquale, V., Levi, T., Goldin, M., Bornat, Y., Tedesco, M., Bisio, M., Kanner, S., Galron, R., Tessadori, J., Taverna, S., Chiappalone, M., 2013. *In vitro* large-scale experimental and theoretical studies for the realization of bi-directional brain-prostheses. Front. Neural Circuits 7, 40.

Bonifazi, P., Ruaro, M.E., Torre, V., 2005. Statistical properties of information processing in neuronal networks. Eur. J. Neurosci. 22(11), 2953–2964.

Bouton, C.E., Shaikhouni, A., Annetta, N.V., Bockbrader, M.A., Friedenberg, D.A., Nielson, D.M., Sharma, G., Sederberg, P.B., Glenn, B.C., Mysiw, W.J., 2016. Restoring cortical control of functional movement in a human with quadriplegia. Nature 533(7602), 247.

Broccard, F.D., Joshi, S., Wang, J., Cauwenberghs, G., 2017. Neuromorphic neural interfaces: from neurophysiological inspiration to biohybrid coupling with nervous systems. J. Neural. Eng. 14(4), 041002.

Bruzzone, A., Pasquale, V., Nowak, P., Tessadori, J., Massobrio, P., Chiappalone, M., 2015. Interfacing in silico and *in vitro* neuronal networks. Conf. Proc. IEEE Eng. Med. Biol. Soc. 2015, 3391–3394.

Chou, Z., Lim, J., Brown, S., Keller, M., Bugbee, J., Broccard, F., Khraiche, M.L., Silva, G.A., Cauwenberghs, G., 2015. Bidirectional neural interface: closed-loop feedback control for hybrid neural systems. Conf. Proc. IEEE Eng. Med. Biol. Soc. 2015, 3949–3952.

Cuppone, A.V., Semprini, M., Konczak, J., 2018. Consolidation of human somatosensory memory during motor learning. Behav. Brain Res. 347, 184–192.

Difato, F., Dal Maschio, M., Marconi, E., Ronzitti, G., Maccione, A., Fellin, T., Berdondini, L., Chieregatti, E., Benfenati, F., Blau, A., 2011. Combined optical tweezers and laser dissector for controlled ablation of functional connections in neural networks. J. Biomed. Opt. 16(5), 051306.

Feigin, V.L., Norrving, B., Mensah, G.A., 2017. Global burden of stroke. Circ. Res. 120(3), 439–448.

Flesher, S.N., Collinger, J.L., Foldes, S.T., Weiss, J.M., Downey, J.E., Tyler-Kabara, E.C., Bensmaia, S.J., Schwartz, A.B., Boninger, M.L., Gaunt, R.A., 2016. Intracortical microstimulation of human somatosensory cortex. Sci. Transl. Med. 8(361), 361ra141.

Forró, C., Thompson-Steckel, G., Weaver, S., Weydert, S., Ihle, S., Dermutz, H., Aebersold, M.J., Pilz, R., Demkó, L., Vörös, J., 2018. Modular microstructure design to build neuronal networks of defined functional connectivity. Biosensors and Bioelectronics 122, 75-87.

Frey, U., Egert, U., Heer, F., Hafizovic, S., Hierlemann, A., 2009. Microelectronic system for high-resolution mapping of extracellular electric fields applied to brain slices. Biosensors and Bioelectronics 24(7), 2191-2198.

Goodman, D.F., Brette, R., 2009. The brian simulator. Front. Neurosci. 3(2), 192–197.

Grassia, F., Kohno, T., Levi, T., 2016. Digital hardware implementation of a stochastic two-dimensional neuron model. J. Physiol. Paris 110(4 Pt A), 409–416.

Greenwald, E., Masters, M.R., Thakor, N.V., 2016. Implantable neurotechnologies: bidirectional neural interfaces--applications and VLSI circuit implementations. Med. Biol. Eng. Comput. 54(1), 1–17.

Guggenmos, D.J., Azin, M., Barbay, S., Mahnken, J.D., Dunham, C., Mohseni, P., Nudo, R.J., 2013. Restoration of function after brain damage using a neural prosthesis. Proc Natl Acad Sci U S A 110(52), 21177-21182.

Habibey, R., Golabchi, A., Latifi, S., Difato, F., Blau, A., 2015. A microchannel device tailored to laser axotomy and long-term microelectrode array electrophysiology of functional regeneration. Lab on a chip 15(24), 4578-4590.

Hayashi, K., Kawai-Hirai, R., Harada, A., Takata, K., 2003. Inhibitory neurons from fetal rat cerebral cortex exert delayed axon formation and active migration *in vitro*. J. Cell Sci. 116(21), 4419–4428.

Hayes, J.P., Bigler, E.D., Verfaellie, M., 2016. Traumatic brain injury as a disorder of brain connectivity. J. Int. Neuropsychol. Soc. 22(2), 120–137.

Hebb, D.O., 1949. The organization of behavior: A neuropsychological approach. John Wiley & Sons.

Hogri, R., Bamford, S.A., Taub, A.H., Magal, A., Del Giudice, P., Mintz, M., 2015. A neuro-inspired model-based closed-loop neuroprosthesis for the substitution of a cerebellar learning function in anesthetized rats. Sci. Rep. 5, 8451.

Izhikevich, E.M., 2003. Simple model of spiking neurons. IEEE Trans. Neural. Netw. 14(6), 1569–1572.

Izhikevich, E.M., 2004. Which model to use for cortical spiking neurons? IEEE Trans. Neural. Netw. 15(5), 1063–1070.

Izhikevich, E.M., Edelman, G.M., 2008. Large-scale model of mammalian thalamocortical systems. Proceedings of the National Academy of Sciences of the United States of America 105(9), 3593–3598.

Javier, G.O., Soriano, J., Alvarez-Lacalle, E., Teller, S., Casademunt, J., 2013. Noise focusing and the emergence of coherent activity in neuronal cultures. Nat. Phys. 9(9), 582.

Johnson, H.A., Goel, A., Buonomano, D.V., 2010. Neural dynamics of *in vitro* cortical networks reflects experienced temporal patterns. Nature Neurosci. 13(8), 917.

Jun, J.J., Steinmetz, N.A., Siegle, J.H., Denman, D.J., Bauza, M., Barbarits, B., Lee, A.K., Anastassiou, C.A., Andrei, A., Aydin, C., Barbic, M., Blanche, T.J., Bonin, V., Couto, J., Dutta, B., Gratiy, S.L., Gutnisky, D.A., Hausser, M., Karsh, B., Ledochowitsch, P., Lopez, C.M., Mitelut, C., Musa, S., Okun, M., Pachitariu, M., Putzeys, J., Rich, P.D., Rossant, C., Sun, W.L., Svoboda, K., Carandini, M., Harris, K.D., Koch, C., O'Keefe, J., Harris, T.D., 2017. Fully integrated silicon probes for high-density recording of neural activity. Nature 551(7679), 232-236.

Jung, R., Brauer, E.J., Abbas, J.J., 2001. Real-time interaction between a neuromorphic electronic circuit and the spinal cord. IEEE Transactions on neural systems and rehabilitation engineering 9(3), 319-326.

Kanner, S., Bisio, M., Cohen, G., Goldin, M., Tedesco, M., Hanein, Y., Ben-Jacob, E., Barzilai, A., Chiappalone, M., Bonifazi, P., 2015. Design, surface treatment, cellular plating, and culturing of modular neuronal networks composed of functionally inter-connected circuits. J. Vis. Exp.(98), doi: 10.3791/52572.

Kipke, D.R., Shain, W., Buzsaki, G., Fetz, E., Henderson, J.M., Hetke, J.F., Schalk, G., 2008. Advanced neurotechnologies for chronic neural interfaces: new horizons and clinical opportunities. J. Neurosci. 28(46), 11830–11838.

Kohler, F., Gkogkidis, C.A., Bentler, C., Wang, X., Gierthmuehlen, M., Fischer, J., Stolle, C., Reindl, L.M., Rickert, J., Stieglitz, T., Ball, T., Schuettler, M., 2017. Closed-loop interaction with the cerebral cortex: a review of wireless implant technology. Brain Comput Interfaces 4(3), 146–154.

Kozai, T.D., Jaquins-Gerstl, A.S., Vazquez, A.L., Michael, A.C., Cui, X.T., 2015. Brain tissue responses to neural implants impact signal sensitivity and intervention strategies. ACS Chem. Neurosci. 6(1), 48–67.

le Feber, J., Erkamp, N., Van Putten, M.J., Hofmeijer, J., 2017. Loss and recovery of functional connectivity in cultured cortical networks exposed to hypoxia. Journal of neurophysiology 118(1), 394-403.

Luczak, A., McNaughton, B.L., Harris, K.D., 2015. Packet-based communication in the cortex. Nat. Rev. Neurosci. 16(12), 745–755.

Maas, A.I.R., Menon, D.K., Adelson, P.D., Andelic, N., Bell, M.J., Belli, A., Bragge, P., Brazinova, A., Buki, A., Chesnut, R.M., Citerio, G., Coburn, M., Cooper, D.J., Crowder, A.T., Czeiter, E., Czosnyka, M., Diaz-Arrastia, R., Dreier, J.P., Duhaime, A.C., Ercole, A., van Essen, T.A., Feigin, V.L., Gao, G., Giacino, J., Gonzalez-Lara, L.E., Gruen, R.L., Gupta, D., Hartings, J.A., Hill, S., Jiang, J.Y., Ketharanathan, N., Kompanje, E.J.O., Lanyon, L., Laureys, S., Lecky, F., Levin, H., Lingsma, H.F., Maegele, M., Majdan, M., Manley, G., Marsteller, J., Mascia, L., McFadyen, C., Mondello, S., Newcombe, V., Palotie, A., Parizel, P.M., Peul, W., Piercy, J., Polinder, S., Puybasset, L., Rasmussen, T.E., Rossaint, R., Smielewski, P., Soderberg, J., Stanworth, S.J., Stein, M.B., von Steinbuchel, N., Stewart, W., Steyerberg, E.W., Stocchetti, N., Synnot, A., Te Ao, B., Tenovuo, O., Theadom, A., Tibboel, D., Videtta, W., Wang, K.K.W., Williams, W.H., Wilson, L., Yaffe, K., In, T.P., Investigators, 2017. Traumatic brain injury: integrated approaches to improve prevention, clinical care, and research. Lancet Neurol. 16(12), 987–1048.

Markram, H., 2012. The human brain project. Sci. Am. 306(6), 50–55.

Melozzi, F., Woodman, M.M., Jirsa, V.K., Bernard, C., 2017. The virtual mouse brain: a computational neuroinformatics platform to study whole mouse brain dynamics. eNeuro 4(3), doi: 10.1523/ENEURO.0111–1517.2017.

Myers, D.K., Goldberg, A.M., Poth, A., Wolf, M.F., Carraway, J., McKim, J., Coleman, K.P., Hutchinson, R., Brown, R., Krug, H.F., 2017. From *in vivo* to *in vitro*: the medical device testing paradigm shift. ALTEX 34(4), 479–500.

Osborn, L.E., Dragomir, A., Betthauser, J.L., Hunt, C.L., Nguyen, H.H., Kaliki, R.R., Thakor, N.V., 2018. Prosthesis with neuromorphic multilayered e-dermis perceives touch and pain. Sci. Robot. 20(9), eaat3818.

Ostry, D.J., Darainy, M., Mattar, A.A., Wong, J., Gribble, P.L., 2010. Somatosensory plasticity and motor learning. J. Neurosci. 30(15), 5384–5393.

Panzeri, S., Harvey, C.D., Piasini, E., Latham, P.E., Fellin, T., 2017. Cracking the Neural Code for Sensory Perception by Combining Statistics, Intervention, and Behavior. Neuron 93(3), 491-507.

Pastore, V.P., Massobrio, P., Godjoski, A., Martinoia, S., 2018. Identification of excitatory-inhibitory links and network topology in large-scale neuronal assemblies from multi-electrode recordings. PLoS computational biology 14(8), e1006381.

Pirog, A., Bornat, Y., Perrier, R., Raoux, M., Jaffredo, M., Quotb, A., Lang, J., Lewis, N., Renaud, S., 2018. Multimed: an integrated, multi-application platform for the real-time recording and sub-millisecond processing of biosignals. Sensors (Basel) 18(7), 2099.

Pizzi, R.M., Rossetti, D., Cino, G., Marino, D., Vescovi, A.L., Baer, W., 2009. A cultured human neural network operates a robotic actuator. Biosystems 95(2), 137–144.

Potter, S.M., 2010. Closing the loop between neurons and neurotechnology. Front. Neurosci. 4, 15.

Roelfsema, P.R., Holtmaat, A., 2018. Control of synaptic plasticity in deep cortical networks. Nat. Rev. Neurosci. 19(3), 166–180.

Rosin, B., Slovik, M., Mitelman, R., Rivlin-Etzion, M., Haber, S.N., Israel, Z., Vaadia, E., Bergman, H., 2011. Closed-loop deep brain stimulation is superior in ameliorating parkinsonism. Neuron 72(2), 370-384.

Shein-Idelson, M., Ben-Jacob, E., Hanein, Y., 2011. Engineered neuronal circuits: a new platform for studying the role of modular topology. Frontiers in neuroengineering 4, 10.

Soekadar, S.R., Birbaumer, N., Slutzky, M.W., Cohen, L.G., 2015. Brain-machine interfaces in neurorehabilitation of stroke. Neurobiol. Dis. 83, 172–179.

Soloperto, A., Bisio, M., Palazzolo, G., Chiappalone, M., Bonifazi, P., Difato, F., 2016. Modulation of neural network activity through single cell ablation: an in vitro model of minimally invasive neurosurgery. Molecules 21(8), 1018.

Steinmetz, N.A., Koch, C., Harris, K.D., Carandini, M., 2018. Challenges and opportunities for large-scale electrophysiology with Neuropixels probes. Curr. Opin. Neurobiol. 50, 92–100.

Takeuchi, N., Izumi, S., 2013. Rehabilitation with poststroke motor recovery: a review with a focus on neural plasticity. Stroke Res. Treat. 2013, 128641.

Thakur, C.S.T., Molin, J., Cauwenberghs, G., Indiveri, G., Kumar, K., Qiao, N., Schemmel, J., Wang, R.M., Chicca, E., Olson Hasler, J., 2018. Large-scale neuromorphic spiking array processors: A quest to mimic the brain. Frontiers in neuroscience 12, 891.

Turrigiano, G.G., 2008. The self-tuning neuron: synaptic scaling of excitatory synapses. Cell 135(3), 422-435.

Valle, G., Mazzoni, A., Iberite, F., D'Anna, E., Strauss, I., Granata, G., Controzzi, M., Clemente, F., Rognini, G., Cipriani, C., Stieglitz, T., Petrini, F.M., Rossini, P.M., Micera, S., 2018. Biomimetic intraneural sensory feedback enhances sensation naturalness, tactile sensitivity, and manual dexterity in a bidirectional prosthesis. Neuron 100(1), 37–45.

Vassanelli, S., Mahmud, M., 2016. Trends and challenges in neuroengineering: toward "intelligent" Neuroprostheses through brain-"brain inspired systems" communication. Front Neurosci. 10, 438.

Wagenaar, D.A., Pine, J., Potter, S.M., 2006. Searching for plasticity in dissociated cortical cultures on multi-electrode arrays. J. Negat. Results Biomed 5, 16.

Wang, W., Collinger, J.L., Perez, M.A., Tyler-Kabara, E.C., Cohen, L.G., Birbaumer, N., Brose, S.W., Schwartz, A.B., Boninger, M.L., Weber, D.J., 2010. Neural interface technology for rehabilitation: exploiting and promoting neuroplasticity. Phys. Med. Rehabil. Clin. N. Am. 21(1), 157–178.

Xu, T., Xiao, N., Zhai, X., Kwan, C.P., Tin, C., 2018. Real-time cerebellar neuroprosthetic system based on a spiking neural network model of motor learning. J. Neural. Eng. 15(1), 016021.

Figure titles and legends

Figure 1. Interfacing a biological neural network and neuromorphic neuroprosthesis. A, Schematic representation of the main elements of the setup: cartoon of an MEA coupled with a BNN; picture of the amplification system; picture of the custom FPGA board; picture of the stimulus generator. Out of the loop, we used a PC to configure the board. **B**, Schematic representation of the different phases of two experimental approaches which share a pre-lesion, a lesion (performed through laser ablation, not shown) and a post lesion phase. The final experimental phase can be either bidirectional bridging (BB) or hybrid bidirectional bridging (HBB). **C**, Schematic of real-time data processing performed by the board: the first step is spike detection followed by network burst (NB) detection monitoring module 1. After NB detection, delivering stimulation to module 2 of the BNN (BB approach) or to the SNN is possible. In the second modality, there is also NB detection of the SNN, which can result in stimulation delivered to the BNN (HBB approach).

Figure 2. A laser ablation-induced lesion can disconnect two neuronal modules. **A1**, Schematic of the first experimental protocol. Experiments with no lesion: we recorded four consecutive hours of spontaneous activity (S1-S4). **A2**, Schematic of the second experimental protocol. Experiments with lesion: we recorded one hour of spontaneous activity (S1) followed by laser ablation and three consecutive hours of spontaneous activity post lesion (SPL1-SPL3). The grey-shaded area indicates 20 minutes of no recording due to the execution of the lesion. **B1,** A 20 s raster plot of the network bursting activity of one representative experiment during the S1 phase. **B2,** a 20 s raster plot of the network bursting activity of one representative experiment during SPL3. **C1**, Cross-correlation (CC) function for one representative experiment during the S1-S4 phases. The CC profiles between the spike trains of each module (light blue) in the four phases of the experiment were high and stable (lines shifted for the sake of clarity). Time axis [-500, +500] ms. **C2**, CC profile between the spike trains of each module for one representative experiment with lesion. Before the lesion (light blue profile), CC was high; following the lesion (dark grey), CC collapsed to zero (lines shifted for the sake of clarity). Time axis [-500, +500] ms. **D1** Percentage of active channels with respect to S1 for

716 the experiments with no lesions (light blue columns, n=9) and with lesions (n=4, dark grey columns).
717 No significant difference was found using the Mann-Whitney test (S2 VS SPL1 p = 0.2042; S3 VS
718 SPL2: p=0.31608; S4 VS SPL3: p=0.70769). **D2,** Mean firing rate (MFR) ratio with respect to S1 for
719 experiments without (light blue bars) and with lesions (dark grey bars). No significant difference was
720 found during the last hour using the Mann-Whitney test (S2 vs SPL1: p = 0.0028; S3 vs SPL2: p =
721 0.01119; S4 vs SPL3: p = 0.10629). **E1,** Comparison of the CC area ratio with respect to S1 for the
722 experiments without (light blue bars) and with lesions (dark grey bars) (Mann-Whitney test; S2 vs
723 SPL1: p =0.0028; S3 vs SPL2: p = 0.0028; S4 vs SPL3: p = 0.0028). **E2,** On the left, comparison of
724 the intra-module correlation coefficient (i.e., Pearson Correlation, PC) ratio with respect to S1 for the
725 experiments without (light blue bars) and with lesions (dark grey bars). No significant difference was
726 found using the Mann-Whitney test (S2 VS SPL1 p = 0.71049; S3 VS SPL2: p= 0.14825; S4 VS
727 SPL3: p= 0.07552). On the right, the same comparison regarding inter-module PC that showed clear
728 differences between experiments without and with lesion (Mann-Whitney test; S2 vs SPL1: p
729 =0.0028; S3 vs SPL2: p = 0.0028; S4 vs SPL3: p = 0.0028). **F1,** Network burst rate (NBR) ratio with
730 respect to S1 showing significant differences during the first and second hour after the lesion (Mann-
731 Whitney test; S2 vs SPL1: p = 0.0028; S3 vs SPL2: p = 0.01119; S4 vs SPL3: p = 0.26014). **F2,**
732 Probability of single-module NB (Prob smNB). The ratio with respect to S1 shows stability for
733 experiments without (light blue bars) and with lesions (dark grey bars) (Mann-Whitney test; S2 vs
734 SPL1: p = 0.0028; S3 vs SPL2: p = 0.0028; S4 vs SPL3: p = 0.0028).
735
736 **Figure 3. Bidirectional bridging is effective in reconnecting functionally and anatomically**
737 **disconnected neuronal modules. A,** Schematic of the experimental protocol. We recorded 20
738 minutes of spontaneous activity (S1) followed by laser ablation. The grey-shaded area indicates 20
739 minutes of no recording during ablation. Dots represent two hours of no recording after the lesion to
740 maintain a stable activity in both modules. Then, we recorded 20 minutes of SPL activity (SPL3)
741 followed by 20 minutes of the bidirectional bridging (BB) protocol and another 20 minutes of
742 spontaneous activity (SPL4). **B1-4**, The 20 s-long raster plots of representative experiments
743 (respectively, from phases S1, SPL1, BB and SPL4). In **B3**, Blue and red lines represent electrical

744 stimulation pulses delivered from module 1 to module 2 and vice versa, respectively. **C**, MFR during
745 the 4 experimental phases was stable (colour code as in panel a: S1: light blue dot; SPL3, SPL4: dark
746 grey dots; BB: red dot). No significant difference was found (one-way RM ANOVA, p=0.469, DF =
747 3, F = 0.872) **D1**, CC function during the 4 experimental phases. Small arrows indicate the blanking
748 period of 8 ms following each stimulation. Colour code the same as that in panel a. Note that during
749 BB, the cross-correlation function (red) recovers even if not completely with respect to the initial
750 profile (light blue), while it stays at zero during the spontaneous activity phases post lesion (SPL3 and
751 SPL4, dark grey profiles). **D2**, CC area was highly reduced during the post-lesion phases. The CC
752 area partially recovered during the BB protocol and collapsed again when stimulation was switched
753 off (one-way repeated measures analysis of variance; degrees of freedom=3; F=101,832. S1 vs SPL3
754 p=5.67E-13; S1 vs SPL4 p=7.54E-13; S1 vs BB p=1.60E-07; BB vs SPL3 p=1.77E-06; BB vs SPL4
755 p=2.81E-06; SPL4 vs SPL3 p=1). **E1**, NBR remained stable during the experiments. No significant
756 difference was found (one-way repeated measures analysis of variance: p=0.501, DF=3; F=0.810).
757 **E2**, Probability of the single-module NB (Prob smNB) was close to one after the lesion. During the
758 BB protocol, the probability was similar to the pre-lesion condition. (Friedman's repeated measures
759 analysis of variance; p<0.001, DF=3, Chi-square=24.3. SPL4 vs S1 and SPL3 vs S1: p<0.001).
760
761 **Figure 4. Spiking neural network (SNN) design and characterization**. **A**, Schematic of the
762 procedure used to create a library of SNNs. Starting from the Izhikevich model implemented on the
763 FPGA and a library of 34 BNNs with a large spectrum of activity, we tuned the mean value of the
764 synaptic weight distribution to obtain and select from a collection of SNNs (SNN library, comprising
765 27 different configurations). **B**, Representative 20 s-long raster plots of different BNNs showing
766 different NB rates. **C**, Left, distribution of excitatory synaptic weights from the 27 SNNs. In red, the
767 slower SNN of the library (SNN 1). The blue arrow indicates the shift of the mean value (from 0.99 to
768 1.34) of the normal distribution with standard deviation = 0.3 to obtain increasing NBR values. Right,
769 distribution of inhibitory synaptic weights from the 27 SNNs. In red, the slower SNN of the library
770 (SNN 1). The blue arrow indicates the shift of the mean value (from -2.02 to -1.02) of the normal
771 distribution with standard deviation = 0.3 to obtain increasing NBR values. **D**. Representative 20 s-

long raster plots of different SNNs showing different NB rates. **E**, Left, cumulative MFR profile for the BNN library. Right, cumulative MFR profile for the SNN library. **F1**, Comparison between BNN and SNN libraries in terms of network MFR (i.e., the mean value of all active electrodes for BNN and neurons for SNN). **F2**, Comparison between BNN and SNN NBR, showing that the SNN library covers the BNN variability and contains networks with a higher NBR.

Figure 5. The hybrid bidirectional bridging approach is effective when a neuronal assembly must be replaced. A, Schematic of the experimental protocols. We recorded 20 minutes of spontaneous activity (S1) followed by laser ablation. Grey-shaded area indicates 20 minutes of no recording during ablation. Dots represent two hours of no recording after the lesion to obtain stable activity in both modules and to test different stimulation channels. Then, we recorded 20 minutes of SPL activity (SPL3) followed by 20 minutes of a hybrid bidirectional bridging (HBB) protocol and another 20 minutes of spontaneous activity (SPL4). **B1,** Top, 20 s-long raster plot depicting the BNN bursting activity involving both modules before lesion. Bottom, activity of SNN uncorrelated with the BNN. The networks are not linked. **B2**, Top, 20 s-long raster plot after lesion showing uncorrelated bursting activity on BNN modules 1 and 2. Bottom, same as that in B1. **B3**, 20 s-long raster plot during HBB depicting two hybrid events. The first event on the left was an NB detected on module 1 of the BNN. The detection resulted in a stimulation pulse delivered to 10 excitatory neurons of the SNN (blue line, bottom). An NB on the SNN was detected 18 ms after the stimulation and triggered the delivery of a stimulation pulse to module 1 of the BNN (grey line, top). **B4,** 20 s-long raster plot depicting the uncorrelated activity of BNN modules (top) and SNN network (bottom). **C,** MFR during the 4 experimental phases was stable (colour code as in panel a: S1: light blue dot; SPL3, SPL4: dark grey dots; HBB: red dot). No significant difference was found (one-way repeated measures analysis of variance. $p<0.001$, DF=3, F=3,16; Bonferroni test: all comparisons with $p>0.05$). **D1,** CC function during the 4 experimental phases. Colour code the same as that in panel **A.** Note that during BB, the cross-correlation function (red) recovers even if not completely with respect to the initial profile (light blue). **D2,** CC area was highly reduced during the post-lesion phases. The CC area partially recovered during the BB protocol and collapsed again when stimulation was switched off (one-way repeated

measures analysis of variance. p<0.001, DF=3; F=70,448; S1 vs SPL3: p=5.80E-10; S1 vs SPL4 p=2.72E-09; S1 vs HBB: p=9.16E-04; HBB vs SPL3 p=1.16E-07; HBB vs SPL4 p=1.02E-06; SPL4 vs SPL3 p=0.73643). **E1,** NBR did not change during HBB with respect to the S1 phase (one-way repeated measures analysis of variance. p=0.005, DF=3; F=6,069; S1 vs SPL3 p=0.02482; S1 vs SPL4 p=1; S1 vs HBB p=1; HBB vs SPL3 p=0.01022; HBB vs SPL4 p=1; SPL4 vs SPL3 p=0.00674). **E2,** Probability of a single-module NB (Prob smNB) was close to one after the lesion. During the HBB protocol, the probability was similar to that in the pre-lesion condition (one-way repeated measures analysis of variance. p<0.001, DF=3; F=453,439; S1 vs SPL3 p=4.96E-13; S1 vs SPL4 p=1.03E-12; S1 vs HBB p=0.22606; HBB vs SPL3 p=1.94E-12; HBB vs SPL4 p=4.30E-12; SPL4 vs SPL3 p=1).

Supplemental video

Performing the lesion, related to Figure 2. Video recorded during a laser ablation of the connections between two modules (visible on the left and right side) of a bimodular cell culture. Video recorded on November 16th 2016. Duration 18s. Link: https://data.mendeley.com/datasets/bnjckk2kht/draft?a=bb802c21-d45c-4c17-be78-34b11d53bed0

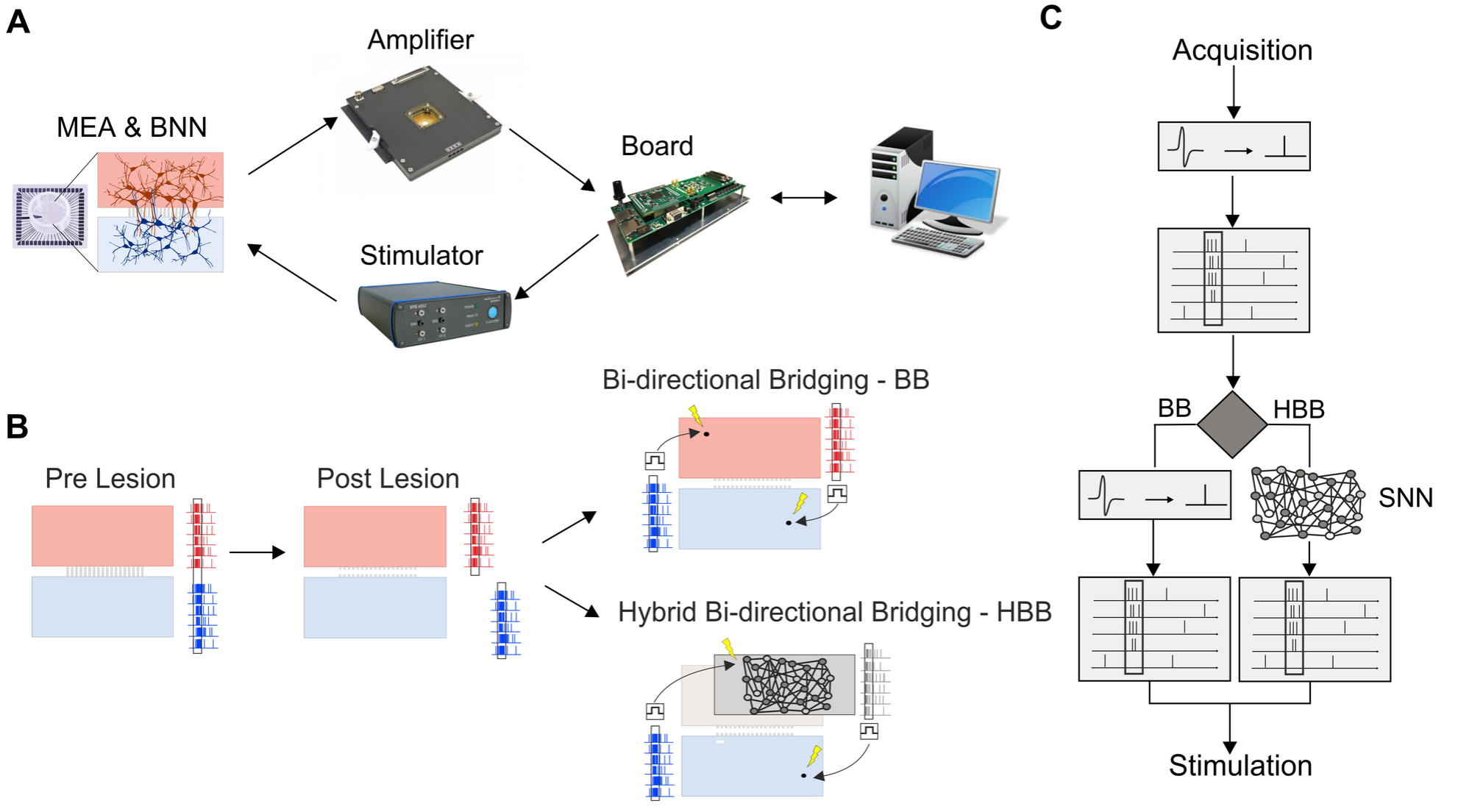
A
Amplifier
MEA & BNN
Board
Stimulator
B
Pre Lesion
Post Lesion
Bi-directional Bridging - BB
Hybrid Bi-directional Bridging - HBB
C
Acquisition
BB
HBB
SNN
Stimulation

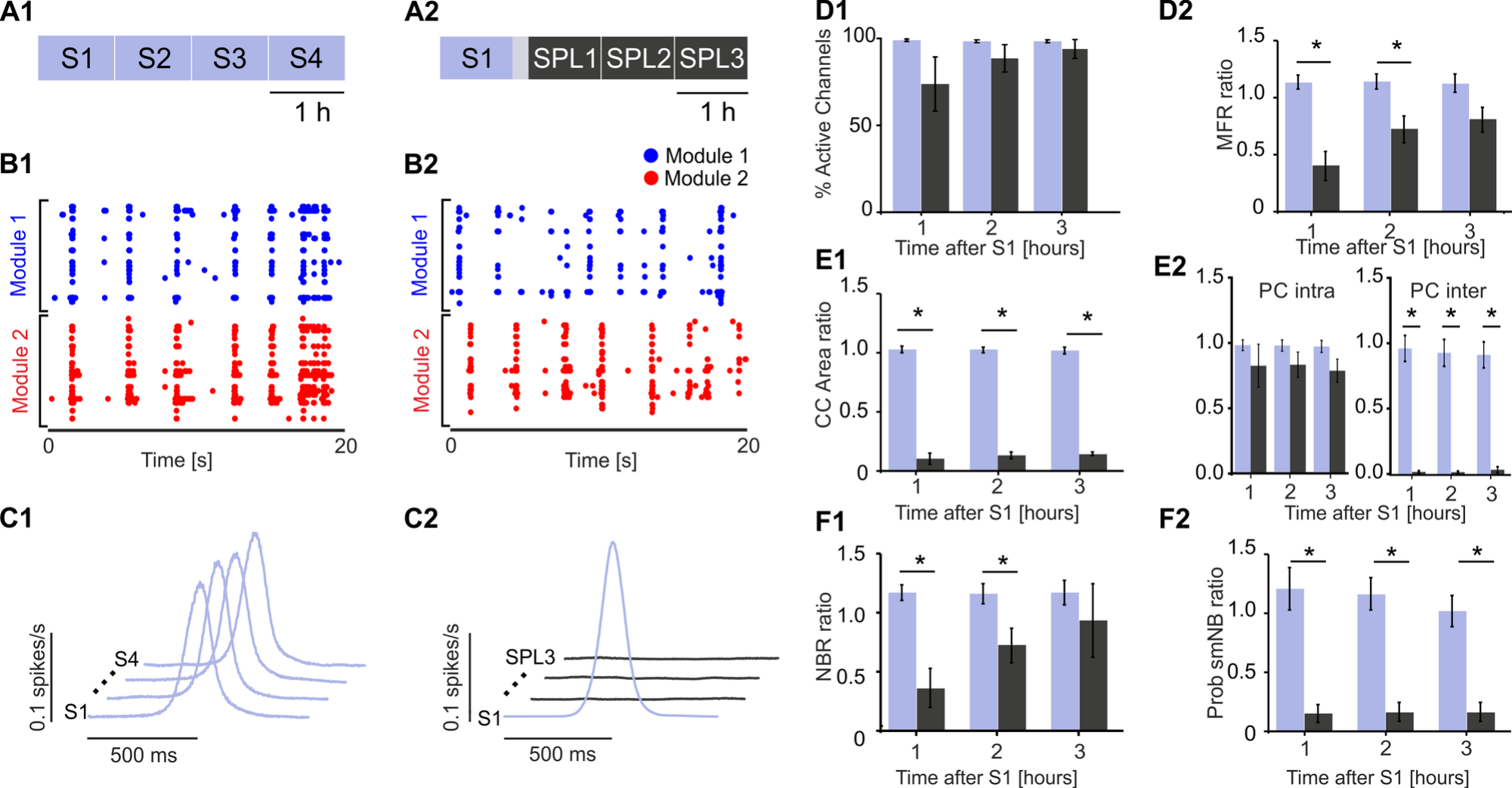
A1
S1
S2
S3
S4
1 h
A2
S1
SPL1
SPL2
SPL3
1 h
B1
Module 1
Module 2
Module 1
Module 2
0
Time [s]
20
B2
Module 1
Module 2
Module 1
Module 2
0
Time [s]
20
C1
0.1 spikes/s
S4
S1
500 ms
C2
0.1 spikes/s
SPL3
S1
500 ms
D1
% Active Channels
100
50
0
1
2
3
Time after S1 [hours]
D2
MFR ratio
1.5
1.0
0.5
0
*
*
1
2
3
Time after S1 [hours]
E1
CC Area ratio
1.5
1.0
0.5
0
*
*
*
1
2
3
Time after S1 [hours]
E2
PC intra
PC inter
1.5
1.0
0.5
0.0
*
*
*
1
2
3
Time after S1 [hours]
F1
NBR ratio
1.5
1.0
0.5
0
*
*
1
2
3
Time after S1 [hours]
F2
Prob smNB ratio
1.5
1.0
0.5
0
*
*
*
1
2
3
Time after S1 [hours]

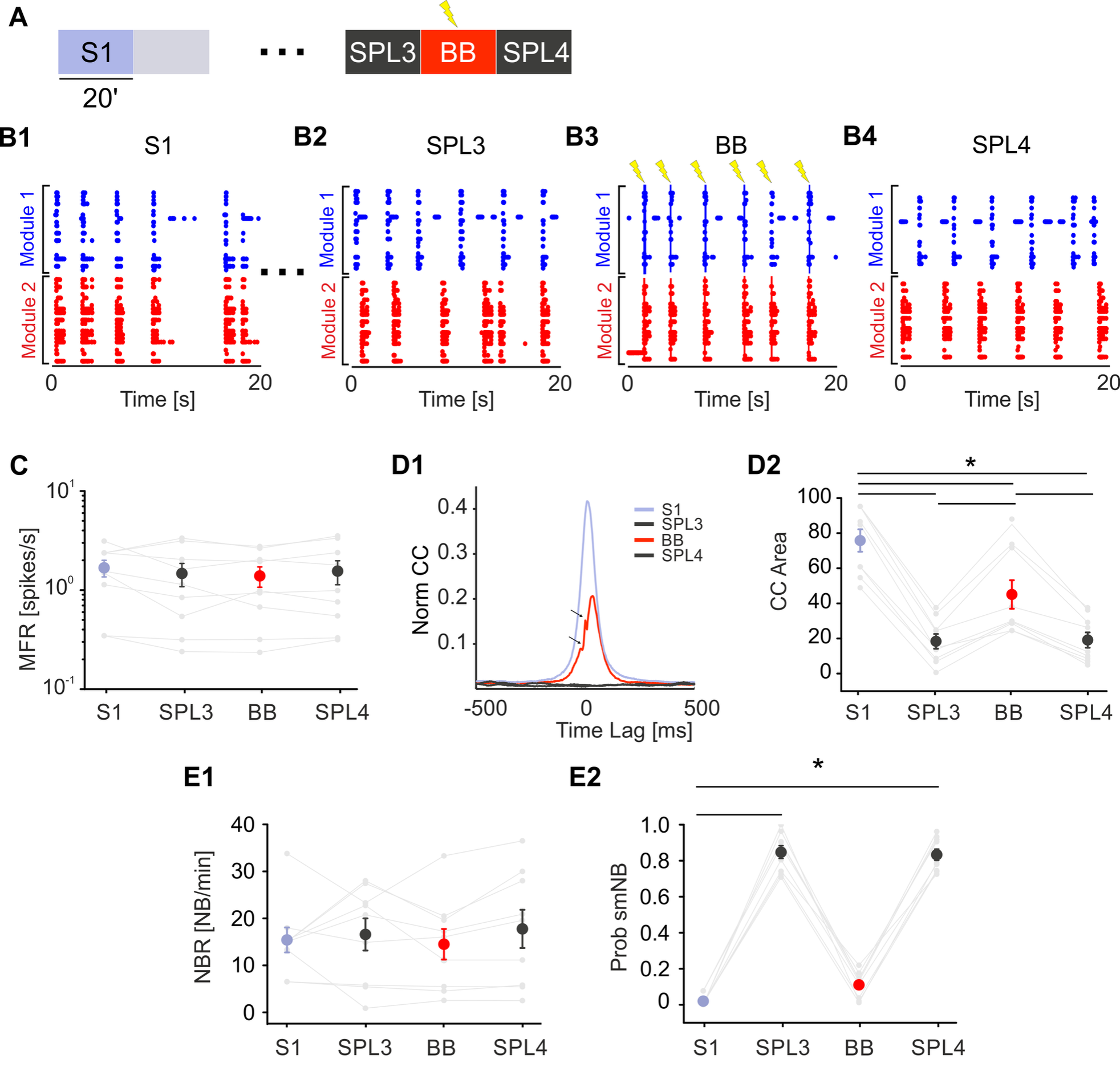
A
S1
SPL3
BB
SPL4
20'
B1
S1
B2
SPL3
B3
BB
B4
SPL4
Module 1
Module 2
0
20
Time [s]
C
MFR [spikes/s]
S1
SPL3
BB
SPL4
D1
Norm CC
S1
SPL3
BB
SPL4
-500
0
500
Time Lag [ms]
D2
CC Area
*
E1
NBR [NB/min]
E2
Prob smNB
*

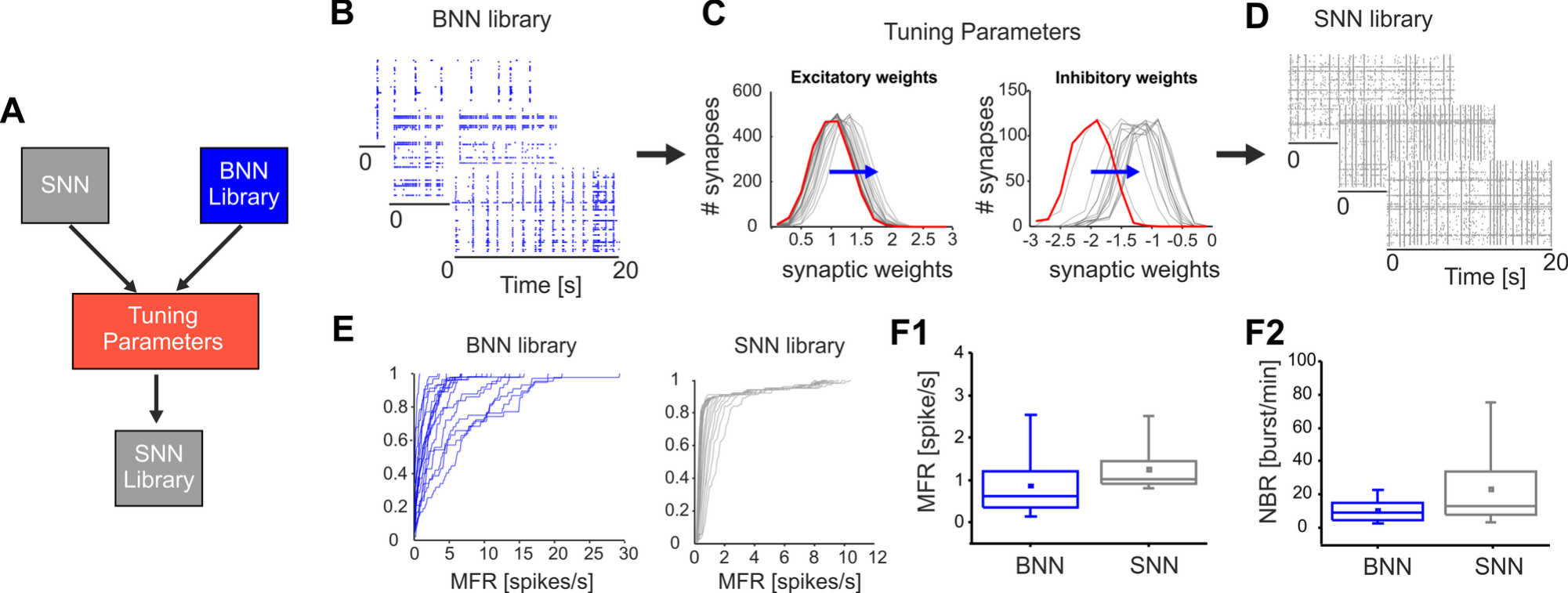
A
SNN
BNN Library
Tuning Parameters
SNN Library
B
BNN library
0
0
0
20
Time [s]
C
Tuning Parameters
Excitatory weights
synapses
600
400
200
0
0.5 1 1.5 2 2.5 3
synaptic weights
Inhibitory weights
synapses
150
100
50
0
-3 -2.5 -2 -1.5 -1 -0.5 0
synaptic weights
D
SNN library
0
0
0
20
Time [s]
E
BNN library
1
0.8
0.6
0.4
0.2
0
0 5 10 15 20 25 30
MFR [spikes/s]
SNN library
1
0.8
0.6
0.4
0.2
0
0 2 4 6 8 10 12
MFR [spikes/s]
F1
MFR [spike/s]
4
3
2
1
0
BNN
SNN
F2
NBR [burst/min]
100
80
60
40
20
0
BNN
SNN

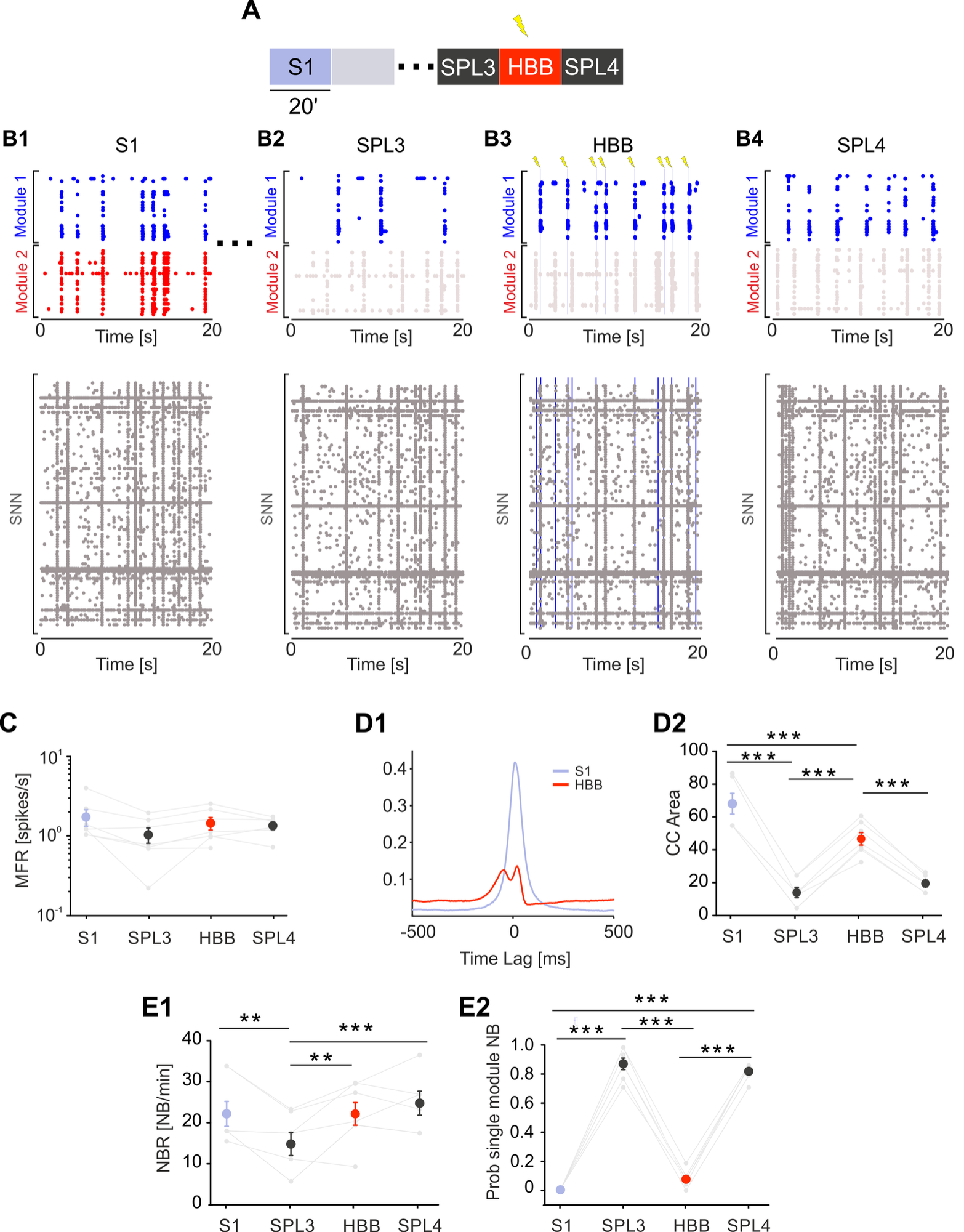
A
S1
SPL3
HBB
SPL4
20'
B1
S1
B2
SPL3
B3
HBB
B4
SPL4
Module 1
Module 2
Time [s]
SNN
C
MFR [spikes/s]
D1
S1
HBB
Time Lag [ms]
D2
CC Area
E1
NBR [NB/min]
E2
Prob single module NB

A Biological Neural Network (BNN) dialoguing in closed-loop with a real-time neuromorphic prosthesis based on a Spiking Neural Network (SNN)

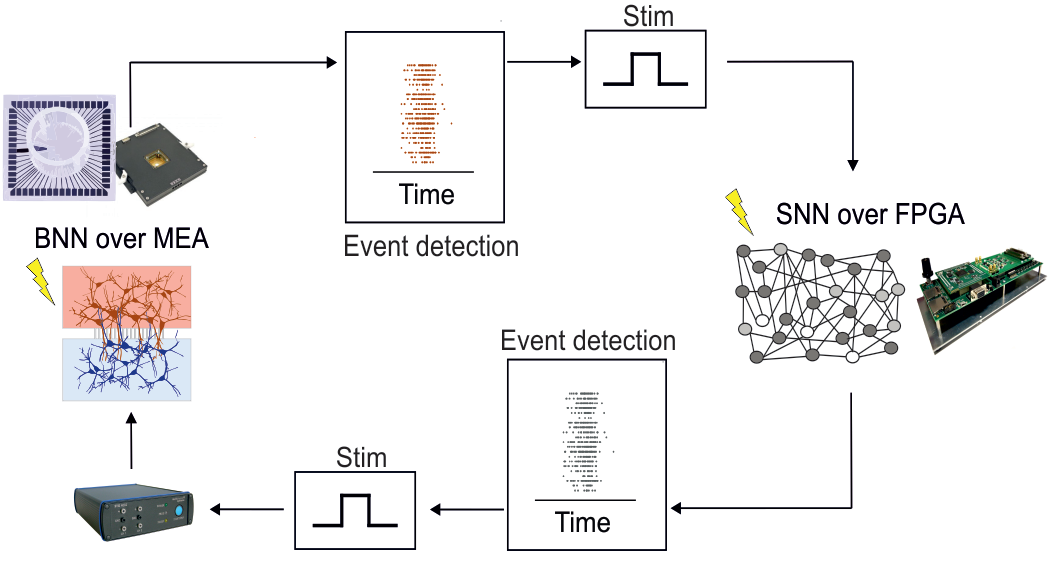

In case of a focal lesion in BNN, the neuromorphic prosthesis can implement two reconnection strategies: Bidirectional Bridging (BB) and Hybrid Bidirectional Bridging (HBB)